Catalysis Communications 35 (2013) 59–63

Contents lists available at SciVerse ScienceDirect

Catalysis Communications

journal homepage: www.elsevier.com/locate/catcom

Short Communication

Selective gas-phase conversion of maleic anhydride to propionic acid on Pt-based catalysts

S.A. Regenhardt, A.F. Trasarti, C.I. Meyer, T.F. Garetto, A.J. Marchi *

Catalysis Science and Engineering Research Group (GICIC), Instituto de Investigaciones en Catálisis y Petroquímica (INCAPE), FIQ-UNL-CONICET, Santiago del Estero 2654 (3000) Santa Fe, Argentina

ARTICLE INFO

Article history:
Received 30 October 2012
Received in revised form 19 December 2012
Accepted 8 February 2013
Available online 15 February 2013

Keywords:
Hydrogenation
Hydrogenolysis
Propionic acid
Platinum supported catalysts

ABSTRACT

Pt-based catalysts, supported on Al_2O_3, SiO_2 and SiO_2–Al_2O_3, were prepared by incipient wetness impregnation and tested in the gas phase hydrogenation of maleic anhydride at atmospheric pressure and 240 °C. In these conditions, the hydrogenolytic activity pattern was: $Pt/SiO_2 > Pt/Al_2O_3 > Pt/SiO_2$–$Al_2O_3$, which is just the opposite of the support acidity trend. These metal Pt-based catalysts showed high selectivity to propionic acid, which was always higher than 80%. The selectivity pattern to this product was: $Pt/Al_2O_3 > Pt/SiO_2 > Pt/SiO_2$–$Al_2O_3$. Both activity and selectivity patterns may be explained on the basis of metal-support interaction and support acidity.

1. Introduction

Propionic acid (PA) is widely employed in the chemical and food industry [1–3]. One use is as food preservative because it inhibits the growth of mold and some kind of bacteria. Another application is in the manufacture of synthetic fibers obtained from cellulose. Some esters derived from PA, such as citronellyl propionate and geranyl propionate, are used as fruit and floral flavors and fragrances. PA salts, such as sodium, calcium and ammonium propionate, are used in veterinary for the treatment of dermatoses, infections and arthritis.

The best known method for obtaining PA is the Reppe process, developed by BASF, consisting in the liquid phase hydrocarboxylation of ethene with carbon monoxide and water, at 200–240 bar and 270–320 °C, employing homogeneous catalysis. The catalyst used in this process is $Ni(CO)_4$ obtained from nickel propionate in the very same reaction medium. The yield in PA, based on ethene, is about 95% [3,4]. This process was improved by Eastman and Halcon by using a Ni/Mo catalyst modified with halogenated and organophosphorus ligands. With this catalyst, it is possible to obtain a similar yield in PA to that one reached in the original process, but now working at 10–35 bar and 175–225 °C [3]. Ethene hydrocarboxylation is also carried out at 170–250 °C and 30–150 bar using a mixture of two metal-based catalysts, e.g. Ni and Pt or Ni and Ru, or bimetallic Ni–Pt or Ni–Ru catalysts [5]. Another method to obtain PA is the ethanol carbonylation, known as Monsanto process, which is carried out in liquid phase with Rh–I catalysts at 75 °C and 28 bar [6]. Other catalysts used in this reaction are based on Rh [7], Co–Ru [8] and Ir [9]. All of these methods use homogeneous catalysis, which requires very sophisticated and expensive methods for product separation and catalyst recycling. With the aim of solving this problem, Ni/C catalysts have been developed to perform heterogeneous catalytic ethanol carbonylation under mild reaction conditions [4,10]. PA is also produced by non-catalytic processes such as microbiological fermentations from lactic acid or glucose [11]. These fermentation processes are tedious and low yields in PA are obtained. The major problem is due to the inhibition of the *Propionibacterium* by acetic acid and PA. In other cases, PA is also obtained as a byproduct from wood distillation.

Gas-phase hydrogenation of maleic anhydride (MA) into succinic anhydride (SA) and its subsequent hydrogenolysis, employing heterogeneous catalysis at low pressure, is an alternative process to produce PA, as shown in Fig. 1. The PA production from MA becomes interesting since this process could be easily integrated to other industrial processes where MA is a byproduct, as for example in the petrochemical industry. To our knowledge, there are no works dealing with this process to obtain PA in high yields. In general, the hydrogenation of MA has been studied with the aim of obtaining SA, γ-butyrolactone (GBL) and/or tetrahydrofurane (THF) [12–18]. In a few cases, yields in PA up to 35% have been reported during the gas phase hydrogenation of MA [19,20].

The aim of this work is to verify the feasibility to convert selectively MA into PA in a one step process using solid Pt-based catalysts in gas

* Corresponding author. Tel.: +54 342 4533858; fax: +54 342 4531068.
E-mail address: amarchi@fiq.unl.edu.ar (A.J. Marchi).

1566-7367/$ – see front matter © 2013 Elsevier B.V. All rights reserved.
http://dx.doi.org/10.1016/j.catcom.2013.02.015

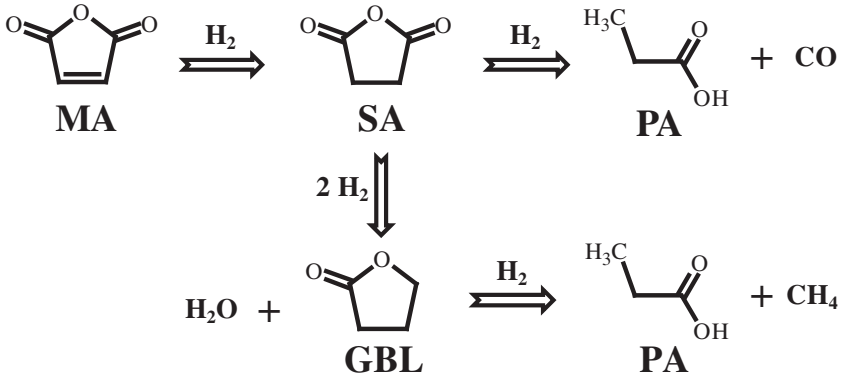

Fig. 1. Reaction network for maleic anhydride (MA) hydrogenation in gas phase. SA: succinic anhydride; PA: propionic acid; GBL: γ-butyrolactone.

phase at atmospheric pressure. In order to determine the influence of the support on the Pt catalytic performance, three different insulating oxides were used: SiO_2, Al_2O_3 and SiO_2–Al_2O_3.

2. Experimental

Pt-supported catalysts were prepared by incipient-wetness impregnation at 25 °C using an aqueous solution of tetramine platinum nitrate, $Pt(NH_3)_4(NO_3)_2$ (99.9%, Alfa), following the procedure described elsewhere [21]. The supports employed in this work were a high purity γ-Al_2O_3 (Cyanamid Ketjen CK 300), SiO_2 (Grace Davison Grade 62) and SiO_2–Al_2O_3 (Sigma-Aldrich, Si/Al = 6.6). The impregnated supports were dried overnight at 100 °C and then calcined in air at 500 °C during 4 h. Finally, these precursors were reduced ex-situ in H_2(100%) flow at 500 °C for 4 h. In a previous work, it was verified that this procedure is enough to ensure that a stable metal Pt phase from complete reduction of platinum oxide can be obtained [21].

The Pt content was measured by ICP (Inductive Coupled Plasma) using a Pelkin Elmer Optima 2100 DV ICP system. Metal dispersion was determined by hydrogen chemisorption at 25 °C. Samples were previously reduced and evacuated at 500 °C. Hydrogen uptake was determined using the double isotherm method in the pressure range 0–6.6 kPa, following the procedure described elsewhere [21]. The specific surface area of the samples obtained after impregnation and calcination was measured by N_2 physisorption at −196 °C using a Quantachrome Autosorb-1 sorptometer and applying BET analysis method. Samples were degassed under vacuum at 250 °C before carrying out the measurements.

Acid site densities were determined by using temperature programmed desorption (TPD) of preadsorbed NH_3. Sample (200 mg) was load in a quartz tubular reactor and then treated at 500 °C for 1.5 h in He flow (~60 cm^3 min^{-1}). Afterwards, the sample was exposed to a stream of NH_3(1%)/He at 100 °C until surface saturation. Physisorbed NH_3 was removed by flowing He at 60 cm^3 min^{-1} for 30 min at 100 °C. Then, the temperature was increased from 100 °C to 600 °C at 10 °C min^{-1}. The NH_3 concentration in the effluent was measured by mass spectrometry (MS) employing a Baltzers Omnistar unit.

Surface acid site nature, i.e. Lewis (L) or Brönsted (B), was determined by Fourier Transform Infrared Spectroscopy (FTIR) of adsorbed pyridine with a Shimadzu FTIR-8101 M spectrophotometer. Sample wafers were initially outgassed at 450 °C for 4 h and then, after cooling up to room temperature, a background spectrum was recorded. Afterwards, pyridine was admitted and adsorbed at room temperature. The spectra were recorded after evacuation at 150 °C for 30 min and cooling again to room temperature. The L/(L + B) ratio was determined deconvolution and integration of the IR absorption bands around 1450 cm^{-1} and 1540 cm^{-1}, assigned to L and B acid sites, respectively [22].

Catalytic activity tests were carried out at atmospheric pressure in a flow set-up equipped with a fixed-bed tubular reactor (SS 1.5 cm i.d.). Catalyst loads (W) of 50 mg and 100 mg, particle size of 0.35–0.42 mm and space times (W/F^0_{MA}) of 12 g h mol^{-1} and 24 g h mol^{-1} were employed in these catalytic experiments. In all of the cases, the catalytic bed was diluted with quartz. Samples, pre-reduced ex-situ in H_2 at 500 °C during 4 h, were load in the tubular reactor and treated in H_2 flow at 300 °C for 1 h, in order to prevent any surface reoxidation of Pt. Afterwards, the reactor was cool down to 240 °C and fed with a stream of H_2 (150 cm^3 min^{-1}) saturated in MA at 80 °C (x_{MA} = 0.0105). On-line analysis of the reactor outlet stream was performed using a Varian CP 3380 gas chromatograph equipped with a flame ionization detector (FID) and a Graphpac GC 0.1% AT-1000 (80–100) packed column.

3. Results and discussion

3.1. Catalyst characterization

Pt content determined by ICP was between 0.4 and 0.5% for all of the samples prepared in this work. After impregnation and calcination, the final specific surface areas were not significantly different from those of the corresponding supports (Table 1), as it was expected due to the low metal loading (<1%) and the impregnation method used. After reduction in H_2 at 500 °C, metallic dispersions varied between 25 and 60%, depending on the support (Table 1). The least dispersed metal phases were obtained when Pt was supported on SiO_2 or SiO_2–Al_2O_3. Instead, a dispersion of about 60% was reached for Pt/Al_2O_3. From these chemisorption data and applying a cubic particle model, medium particle sizes between 1.5 and 3.5 nm were estimated (Table 1). These values are indicating that very small metal particles are formed on the supports used in this work.

Surface acid sites concentrations were estimated by deconvolution and integration of NH_3 desorption profiles obtained in TPD-NH_3 experiments (Fig. 2 and Table 1). No NH_3 desorption was detected

Table 1
Physicochemical characterization of samples calcined in air at 400 °C.

Sample	Sg[a] (m^2 g^{-1})	D[b] (%)	d_p[c] (nm)	NH_3 TPD (μmol g^{-1})	NH_3 TPD (μmol m^{-2})	L/(L + B)[d]
SiO_2	254	–	–	n.d.	n.d.	–
γ-Al_2O_3	190	–	–	21	0.11	1
SiO_2–Al_2O_3	467	–	–	560	1.20	0.75
Pt/SiO_2	250	24	3.5	n.d.	n.d.	–
Pt/Al_2O_3	188	60	1.4	24	0.13	–
Pt/SiO_2–Al_2O_3	433	25	3.4	537	1.24	–

[a] Sg: specific surface area.
[b] D: metallic dispersion.
[c] d_p: Metal particle size assuming cubic geometry.
[d] L/(L + B): Lewis (L) sites fraction respect to Brönsted (B) sites determined by infrared spectroscopy of absorbed pyridine.

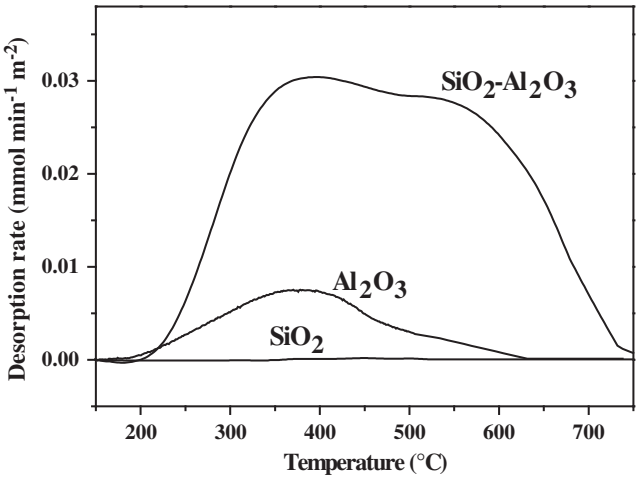

Fig. 2. TPD-NH_3 profiles ($m/e = 16$) for the supports used in this work (NH_3 adsorption at 100 °C and desorption at 10 °C min^{-1}).

in the case of SiO_2 and Pt/SiO_2. The total amount of NH_3 desorbed by mass unit from SiO_2–Al_2O_3 was about 25 times higher than that one desorbed from Al_2O_3. On an areal basis, the acid site density on SiO_2–Al_2O_3 surface was almost 11 times higher than one on Al_2O_3. Besides, SiO_2–Al_2O_3 showed approximately 40% of NH_3 desorbing above 500 °C, while the main NH_3 desorption from Al_2O_3 occurred below 500 °C (Fig. 2). Thus, SiO_2–Al_2O_3 showed higher acid site density and acid sites of higher strength than Al_2O_3. The total density of acid sites for Pt/SiO_2–Al_2O_3 and Pt/Al_2O_3 were similar to those on SiO_2–Al_2O_3 and Al_2O_3, respectively (Table 1). These results are indicating that the incorporation of low Pt loads, i.e. 0.4–0.5%, did not significantly modify the strength and acid site density on the support surface.

From the results obtained by TPD-NH_3 and FTIR of adsorbed pyridine (Table 1), it can be inferred that γ-Al_2O_3 has a low concentration of Lewis acid sites on its surface. Instead, SiO_2–Al_2O_3 contains both Lewis and Brönsted acid sites, with prevalence of Lewis acid sites, and a significant concentration of strong acid sites.

3.2. Catalytic test

In the conditions used in this work, 240 °C and $W/F^0_{MA} = 12$ and 24 g h mol^{-1}, complete and fast hydrogenation of MA into SA was reached with all of the Pt-based catalysts. Then, SA was converted by hydrogenolysis into GBL and PA [19,20]. This is in agreement with the fact that metal Pt promotes hydrogenation of C=C bonds more easily than hydrogenation and hydrogenolysis of a C=O group [23]. At 240 °C and $W/F^0_{MA} = 12$ g h mol^{-1}, the SA conversion on Pt/SiO_2 diminished from 83% up to 68%, reaching a steady state after 100 min. The initial SA conversion and the conversion decay with time were lower with Pt/Al_2O_3 and Pt/SiO_2–Al_2O_3 than with Pt/SiO_2 (Fig. 3A, Table 2). At $W/F^0_{MA} = 24$ g h mol^{-1}, the SA conversion with Pt/SiO_2 reached 100% and remained constant during the 3 h run (Fig. 3B, Table 2). Instead, the initial SA conversion with Pt/Al_2O_3 was almost 94% but decreased up to a final value of 73%. Similarly, SA conversion with Pt/SiO_2–Al_2O_3 decreased almost linearly from 70 to 55% during the 3 h activity test.

In summary, all catalysts were active for SA hydrogenolysis and the activity pattern was: $Pt/SiO_2 > Pt/Al_2O_3 > Pt/SiO_2$–$Al_2O_3$. Then, it is proposed that the Pt hydrogenolytic activity diminished as density and strength of acid sites on support surface increased. It is likely that the electronic properties of the small metal Pt particles were affected by the intimate interaction with the support acid and basic sites. It is very well known that this interaction on Al_2O_3 and SiO_2–Al_2O_3 is occurring from the impregnation step: by adsorption of $Pt(NH_3)_4^{2+}$ ions on

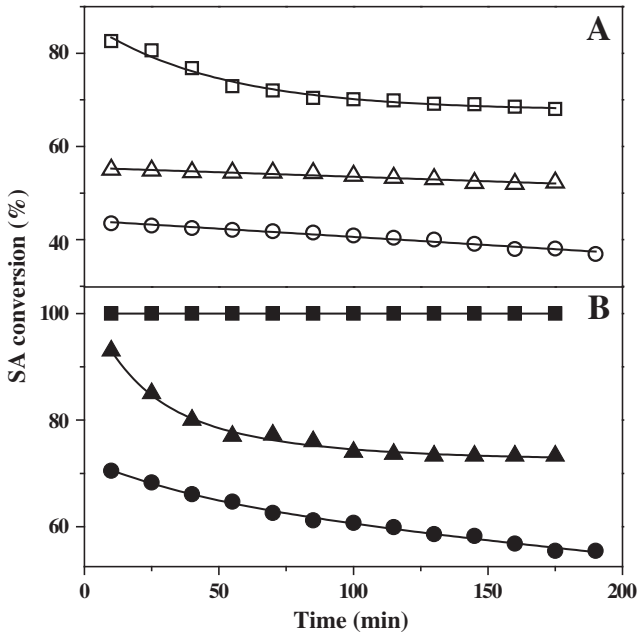

Fig. 3. Conversion of succinic anhydride (SA) as a function of time at 240 °C and 1 bar. (A) $W/F^0_{MA} = 12$ g h mol^{-1}, □ Pt/SiO_2, Δ Pt/Al_2O_3, ○ Pt/SiO_2–Al_2O_3; (B) $W/F^0_{MA} = 24$ g h mol^{-1}, ■ Pt/SiO_2, ▲ Pt/Al_2O_3, ● Pt/SiO_2–Al_2O_3.

Al_2O_3 basic sites and by cation exchange with H^+ on SiO_2–Al_2O_3 strong acid sites. Instead, neither basic sites nor strong acid sites were detected on SiO_2 surface and so the Pt-support interaction must be the lowest of this catalyst series. Thus, Pt-support interaction with acid and basic sites is probably leading to a metal Pt phase less active for SA hydrogenolysis into PA and GBL than the one formed on Pt/SiO_2.

When $W/F^0_{MA} = 12$ g h mol^{-1}, deactivation of Pt/SiO_2 for SA hydrogenolysis was observed (Fig. 3A). This deactivation is likely due to strong irreversible adsorption of reactant and/or product molecules on the metal active sites [13]. Sintering was discarded as a deactivation cause since: 1) metal Pt phase was stabilized during the calcination–reduction process; 2) hydrogenolysis rate of cyclic compounds is higher on large particles and then activity should increase with sintering. At similar conditions, the deactivation was less important for those catalysts with higher acid site density, i.e. Pt/Al_2O_3 and Pt/SiO_2–Al_2O_3. It is probably that the irreversible adsorption of reactant or product molecules on metal Pt was lower with Pt/Al_2O_3 and Pt/SiO_2–Al_2O_3 than with Pt/SiO_2. The last is probably due to the same reasons given above to explain the lower catalyst activity for SA hydrogenolysis as support

Table 2
Hydrogenolytic activity and selectivity of Pt-supported catalysts at different space times (T = 240 °C; P = 1 atm).

Sample	W/F^0_{MA} (g h mol^{-1})	Time (min)	X_{SA}[a] (%)	S_{PA}[b] (%)	Y_{PA}[c] (%)	Y_{GBL}[c] (%)	Y_{CH4}[c] (%)
Pt/SiO_2	12	10	82.6	84.8	67.0	12.0	3.6
		180	68.1	85.1	57.9	10.2	0.0
	24	10	100	86.2	85.0	13.6	1.4
		180	100	88.8	87.0	11.0	2.0
Pt/Al_2O_3	12	10	55.0	95.7	51.5	2.3	1.2
		180	52.0	97.6	48.3	1.2	2.5
	24	10	94.0	95.6	86.5	4.0	3.5
		180	73.3	97.7	69.3	1.6	2.4
Pt/SiO_2–Al_2O_3	12	10	41.3	84.7	29.9	5.4	6.0
		180	34.2	92.4	29.0	2.4	2.8
	24	10	70.0	76.0	33.3	9.9	26.8
		180	55.5	82.1	32.5	7.1	15.9

[a] X_{SA}: Succinic anhydride (SA) conversion.
[b] S_{PA}: Selectivity to propionic acid (PA) defined as $Y_{PA}/(Y_{PA} + Y_{GBL})$.
[c] Yi: Product yield as mol of product (i) by mol of maleic anhydride (MA) fed.

acidity increased. The deactivation of metal sites on Pt/Al_2O_3 and $Pt/SiO_2–Al_2O_3$ became more important when $W/F^0_{MA} = 24$ g h mol^{-1}. It is probably that some compounds were slowly formed on the support acid sites, at the metal-support interface, which then migrated to the metal surface deactivating Pt sites. Thus, the deactivation of metal Pt sites on Pt/Al_2O_3 and $Pt/SiO_2–Al_2O_3$ became more important as the space time increase. This last deactivation mechanism is not probably taking place in the case of Pt/SiO_2.

The only products detected from SA hydrogenolysis were PA, GBL and CH_4, in agreement with reaction scheme shown in Fig. 1. It is worth to notice that in all of the cases, metal Pt resulted highly selective to PA (Table 2), in contrast with other non-noble metal catalysts tested in previous works [12–18]. Selectivity to PA at t = 10 min, for $W/F^0_{MA} =$ 12 g h mol^{-1}, followed the pattern Pt/Al_2O_3 (96%) > $Pt/SiO_2–Al_2O_3$ (85%) ≅ Pt/SiO_2 (85%). Instead, for a $W/F^0_{MA} = 24$ g h mol^{-1}, the selectivity pattern was Pt/Al_2O_3 (96%) > Pt/SiO_2 (86%) > $Pt/SiO_2–Al_2O_3$ (76%). For both space times, the selectivity to PA remained almost constant during the 3 h run with both Pt/SiO_2 and Pt/Al_2O_3, while it increased slightly on $Pt/SiO_2–Al_2O_3$. Thus, the highest selectivity to PA was reached when the metal Pt phase was interacting with the γ-Al_2O_3 surface.

For $W/F^0_{MA} = 12$ g h mol^{-1}, the PA, GBL and CH_4 production rates and yields with Pt/SiO_2 diminished monotonically with time, until a steady state was reached (Fig. 4). These trends were similar to that observed for SA conversion (Fig. 3). This is in agreement with the fact that metal sites, active for SA hydrogenolysis reactions, are deactivated with time. This deactivation is probably due to strong adsorption of reactant and/or product molecules on metal Pt sites, as it was suggested above and in previous works [13,19]. In the case of Pt/Al_2O_3, PA and GBL production rates followed similar trends to that determined for SA conversion, i.e. a linear slight decrease with time indicating a very slow deactivation of metal hydrogenolytic sites. However, CH_4 production rate showed exactly the opposite trend. Finally, with $Pt/SiO_2–Al_2O_3$, PA production rate kept practically constant. Instead, GBL production rate decreased slowly with time, with a similar linear trend to that observed for SA conversion, while CH_4 production rate diminished exponentially to reach a steady state after 1 h. The product evolutions observed with Pt/Al_2O_3 and $Pt/SiO_2–Al_2O_3$, are indicating that PA and GBL are most probably coming from parallel SA hydrogenolysis on different types of metal Pt sites (Fig. 1). Instead, CH_4 was not only a GBL hydrogenolysis product but was also coming from a side reaction no depicted in Fig. 1.

When $W/F^0_{MA} = 24$ g h mol^{-1}, with Pt/SiO_2, PA production rate remains constant at 100% SA conversion (Fig. 5). However, GBL production rate decreased with time, indicating a deactivation of hydrogenolytic metal sites similar to that observed at $W/F^0_{MA} = 12$ g h mol^{-1}. With Pt/Al_2O_3, PA, GBL and CH_4 production rates and yields diminished with time (Table 2, Fig. 5). Instead, with $Pt/SiO_2–Al_2O_3$, PA production rate remains almost constant during the 3 h run, while GBL diminished with time. This is again indicating that SA hydrogenolysis is taking place on two different types of metallic hydrogenolytic sites, similarly to that observed in previous works [19,20]. The relative surface concentration of metal sites that are selective for SA hydrogenolysis into PA respect to those selective to GBL increased as the metal Pt dispersion was higher (Tables 1 and 2). On the other hand, the high CH_4 production rate with $Pt/SiO_2–Al_2O_3$ and its rapid decrease with time are again indicating that CH_4 is mainly coming from a side reaction not shown in Fig. 1. It is very likely that at the beginning SA was adsorbed on both metal Pt and strong acid sites of the support. The SA adsorbed on metal Pt sites reacted following the parallel and series reactions represented in Fig. 1. Instead, SA adsorbed on the strongest Lewis and Brönsted acid sites was converted into CH_4 and other carbonaceous fragments. Then, CH_4 desorbed while the carbonaceous fragments remained strongly adsorbed on the $SiO_2–Al_2O_3$ surface, blocking the strong Lewis acid sites. Thus, total SA conversion was due to hydrogenolysis reactions on metal sites (Fig. 1) and some hydrocracking reactions on strong acid sites present on $SiO_2–Al_2O_3$ surface. As a consequence of the blockage of strong acid sites, total SA conversion and CH_4 production rate diminished with time while PA production rate remained almost constant. Meanwhile, GBL production rate diminished slowly due to strong adsorption of reactant and/or product molecules on metal Pt hydrogenolytic sites, similarly to what happened for Pt/SiO_2, with low or none acidity.

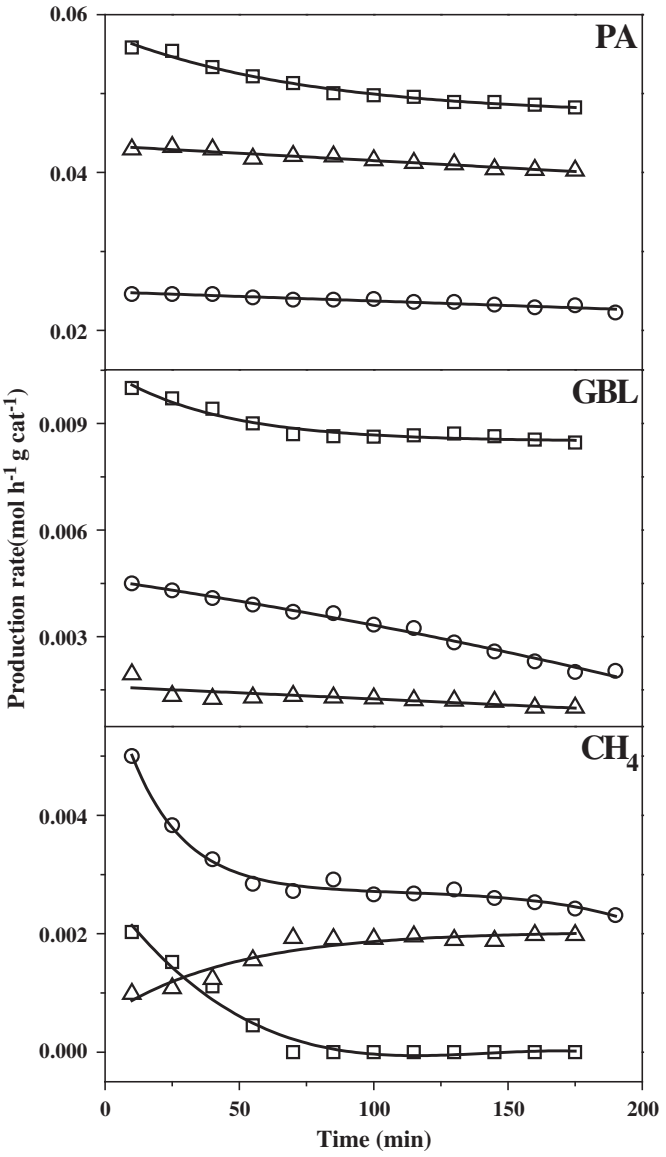

Fig. 4. Production rates of propionic acid (PA), γ-butyrolactone (GBL) and CH_4 at 240 °C, 1 bar and $W/F^0_{MA} = 12$ g h mol^{-1}. □ Pt/SiO_2, Δ Pt/Al_2O_3, ○ $Pt/SiO_2–Al_2O_3$.

4. Conclusions

Propionic acid can be synthesized via gas-phase hydrogenation of maleic anhydride to succinic anhydride on Pt-supported catalysts using a single reactor system, at atmospheric pressure and low space times. High activity in the selective hydrogenolysis of succinic anhydride is obtained when the support has low acidity and Pt-support interaction is weak. Increasing acidity and metal-support interaction lead to a diminution in metal activity and to an increase in methane yield. Thus, the highest yield in propionic acid is obtained with Pt/SiO_2, having the lowest support acidity and the weakest Pt-support interaction of the catalyst series used in this work.

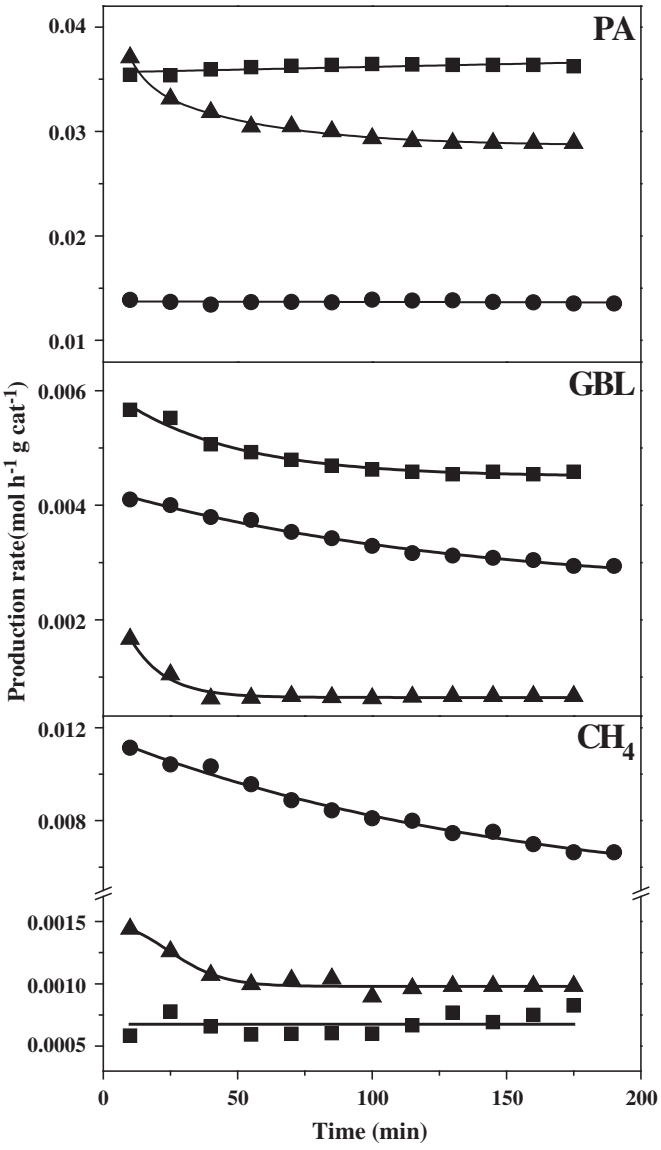

Fig. 5. Production rates of propionic acid (PA), γ-butyrolactone (GBL) and CH_4 at 240 °C, 1 bar and $W/F^0_{MA} = 24$ g h mol^{-1}. ■ Pt/SiO_2, ▲ Pt/Al_2O_3, ● Pt/SiO_2–Al_2O_3.

Acknowledgments

We thank the Universidad Nacional del Litoral (UNL), Consejo Nacional de Investigaciones Científicas y Técnicas (CONICET) and Agencia Nacional de Promoción Científica y Tecnológica (ANPCyT), Argentina, for the financial support to this project.

References

[1] S.J. Zhang, Y.Q. Fang, W.J. Zhao, X.F. Li, Journal of Fuel Chemistry and Technology 17 (4) (1989) 316–321.
[2] D. Foster, T.C. Singleton, Journal of Molecular Catalysis 17 (1982) 299–314.
[3] K. Weissermel, H.-J. Arpe, Industrial Organic Chemistry, fourth ed., Wiley-VCH, 2003.
[4] Q. Zhang, H. Wang, G. Sun, K. Huang, W. Fang, Y. Yang, Journal of Natural Gas Chemistry 17 (2008) 355–358.
[5] F. Lippert, A. Höhn, M. Schäfer, L. Hupfer, US Patent 5 705 683, 1998.
[6] J. Roth, J.H. Craddock, A. Hershman, F.E. Paulik, Chemical Technology 23 (1971) 600–605.
[7] R.P. Patil, A.A. Kelkar, R.V. Chaudari, Journal of Molecular Catalysis 47 (1988) 87–97.
[8] G. Jenner, P. Andrianary, Journal of Catalysis 103 (1987) 37–45.
[9] R.P. Patil, A.A. Kelkar, R.V. Chaudhari, Journal of Molecular Catalysis 72 (1992) 153–165.
[10] X.X. Guan, W.J. Zhao, Industrial Catalysis 7 (1999) 23–27.
[11] S.A. Woskow, B.A. Glatz, Applied and Environmental Microbiology 57 (1991) 2821–2828.
[12] M. Messori, A. Vaccari, Journal of Catalysis 150 (1994) 177–185.
[13] C.I. Meyer, A.J. Marchi, A. Monzón, T.F. Garetto, Applied Catalysis A 367 (2009) 122–129.
[14] J. Li, W.P. Tian, X. Wang, L. Shi, Chemical Engineering Journal 175 (2011) 417–422.
[15] Y. Yu, Y. Guo, W. Zhan, Y. Guo, Y. Wang, Y. Wang, Z. Zhang, G. Lu, Journal of Molecular Catalysis A 337 (2011) 77–81.
[16] D. Zhang, H. Yin, Ch. Ge, J. Xue, T. Jiang, L. Yu, Y. Shen, Journal of Industrial and Engineering Chemistry 15 (2009) 537–543.
[17] Q. Wang, H. Cheng, R. Liu, J. Hao, Y. Yu, F. Zhao, Catalysis Today 148 (2009) 368–372.
[18] Q. Wang, H. Cheng, R. Liu, J. Hao, Y. Yu, Sh. Cai, F. Zhao, Catalysis Communications 10 (2009) 592–595.
[19] C.I. Meyer, S.A. Regenhardt, A.J. Marchi, T.F. Garetto, Applied Catalysis A 417–418 (2012) 59–65.
[20] S.A. Regenhardt, C.I. Meyer, T.F. Garetto, A.J. Marchi, Applied Catalysis A 449 (2012) 81–87.
[21] T.F. Garetto, E. Rincón, C.R. Apesteguía, Applied Catalysis B: Environmental 48 (2004) 167–174.
[22] G. Busca, Catalysis Today 41 (1998) 191–206.
[23] M.A. Vannice, B. Sen, Journal of Catalysis 115 (1989) 65–78.